

# EMM EMUS Observations of Hot Oxygen Corona at Mars: Radial Distribution and Temporal Variability

Krishnaprasad Chirakkil<sup>1,2,3</sup>, Justin Deighan<sup>1</sup>, Michael S. Chaffin<sup>1</sup>, Sonal K. Jain<sup>1</sup>, Robert J. Lillis<sup>3</sup>, Susarla Raghuram<sup>1,2</sup>, Greg Holsclaw<sup>1</sup>, David A. Brain<sup>1</sup>, Ed Thiemann<sup>1</sup>, Phil Chamberlin<sup>1</sup>, Matthew O. Fillingim<sup>3</sup>, J. Scott Evans<sup>4</sup>, Scott England<sup>5</sup>, Hessa AlMatroushi<sup>6</sup>, Hoor AlMazmi<sup>7</sup>, Frank Eparvier<sup>1</sup>, Marko Gacesa<sup>2,8</sup>, Nayla El-Kork<sup>2,8</sup>, Shannon M. Curry<sup>3,1</sup>

<sup>1</sup>Laboratory for Atmospheric and Space Physics, University of Colorado Boulder, Boulder, CO, USA

<sup>2</sup>Space and Planetary Science Center, Khalifa University, Abu Dhabi, UAE

<sup>3</sup>Space Sciences Laboratory, University of California, Berkeley, CA, USA

<sup>4</sup>Computational Physics Inc., Springfield, VA, USA

<sup>5</sup>Department of Aerospace and Ocean Engineering, Virginia Polytechnic Institute and State University, Blacksburg, VA, USA

<sup>6</sup>Mohammed Bin Rashid Space Centre, Dubai, UAE

<sup>7</sup>United Arab Emirates Space Agency, Abu Dhabi, UAE

<sup>8</sup>Department of Physics, Khalifa University, Abu Dhabi, UAE

## Key Points:

- Brighter O corona is observed during perihelion and dimmer during aphelion (with a ratio of  $\sim 4.5$ ), indicating a strong relationship with the Sun–Mars distance
- The variation in OI 130.4 nm brightness shows a linear correlation with solar EUV irradiance, with a short–term solar rotation periodicity
- Interannual variability is observed from MY 36 to MY 37, showing an enhancement in O corona brightness with the rise of Solar Cycle 25

February 3, 2024

---

Corresponding author: Krishnaprasad Chirakkil, [krishnaprasad.chirakkil@lasp.colorado.edu](mailto:krishnaprasad.chirakkil@lasp.colorado.edu), [kpchirakkil@gmail.com](mailto:kpchirakkil@gmail.com)

## Abstract

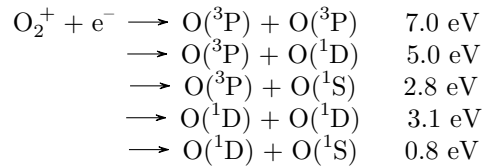
We present the first observations of the dayside coronal oxygen emission in far ultraviolet (FUV) measured by the Emirates Mars Ultraviolet Spectrometer (EMUS) onboard the Emirates Mars Mission (EMM). The high sensitivity of EMUS is providing an opportunity to observe the tenuous oxygen corona in FUV, which is otherwise difficult to observe. Oxygen resonance fluorescence emission at 130.4 nm provides a measurement of the upper atmospheric and exospheric oxygen. More than 500 oxygen corona profiles are constructed using the long-exposure time cross-exospheric mode (OS4) of EMUS observations. These profiles range from  $\sim 200$  km altitude up to several Mars radii ( $>6 R_M$ ) across all seasons and for two Mars years. Our analysis shows that OI 130.4 nm is highly correlated with solar irradiance (solar photoionizing and 130.4 nm illuminating irradiances) as well as changes in the Sun-Mars distance. The prominent short term periodicity in oxygen corona brightness is consistent with the solar rotation period (quasi-27-days). A comparison between the perihelion seasons of Mars Year (MY) 36 and MY 37 shows interannual variability with enhanced emission intensities during MY 37, due to the rise of Solar Cycle 25. These observations show a highly variable oxygen corona, which has significant implications on constraining the photochemical escape of atomic oxygen from Mars.

## Plain Language Summary

The highly sensitive Emirates Mars Ultraviolet Spectrometer (EMUS) onboard Emirates Mars Mission (EMM) is capable of observing ultraviolet emissions emanating from Mars. Oxygen in Martian exosphere is hard to see because it's tenuous. In this study, the analysis of the long exposure time EMUS optical observations show that the hot oxygen corona on Mars has a short term variability due to solar rotation. Hot oxygen corona also shows a long-term variability that depends on the Sun-Mars distance and the solar cycle progression. When comparing data from two Martian years, it is noticed that the oxygen corona became brighter when the Sun is more active.

## 1 Prior Studies of the Hot Oxygen Corona at Mars

Atomic oxygen in the Martian atmosphere is produced by the photodissociation of atmospheric carbon dioxide (Nier & McElroy, 1977; Barth et al., 1971; Ip, 1988, 1990). Atomic oxygen is the dominant neutral species in the Martian upper atmosphere, and quantifying its loss budget is important for understanding the evolution of CO<sub>2</sub> and H<sub>2</sub>O reservoirs at Mars (Deighan et al., 2015). Oxygen in the collisional thermosphere and lower exosphere is called thermal (or cold) oxygen, while that in the upper exosphere (above  $\sim 600$  km) is called non-thermal (or hot) oxygen. Dissociative recombination of O<sub>2</sub><sup>+</sup> in the ionosphere is the primary source of hot oxygen atoms, and hence this reaction is an important loss mechanism for oxygen from Mars (McElroy, 1972; Lillis et al., 2017). Dissociative recombination of O<sub>2</sub><sup>+</sup> can take place via five channels (Fox & Hać, 2009; Kim et al., 1998):



The mean excess energy released in the dissociative recombination channels is equally shared between the two newly formed oxygen atoms. The first two channels, which are highly exothermic, results in oxygen atoms having enough energy (more than the escape energy of  $\sim 2$  electron volts at exobase) to escape the gravitational pull of the planet. The output of the third channel has been found to be minimal, while the last two channels are dependent on the vibrational state of O<sub>2</sub><sup>+</sup> (Petrignani et al., 2004). The characteristic energy

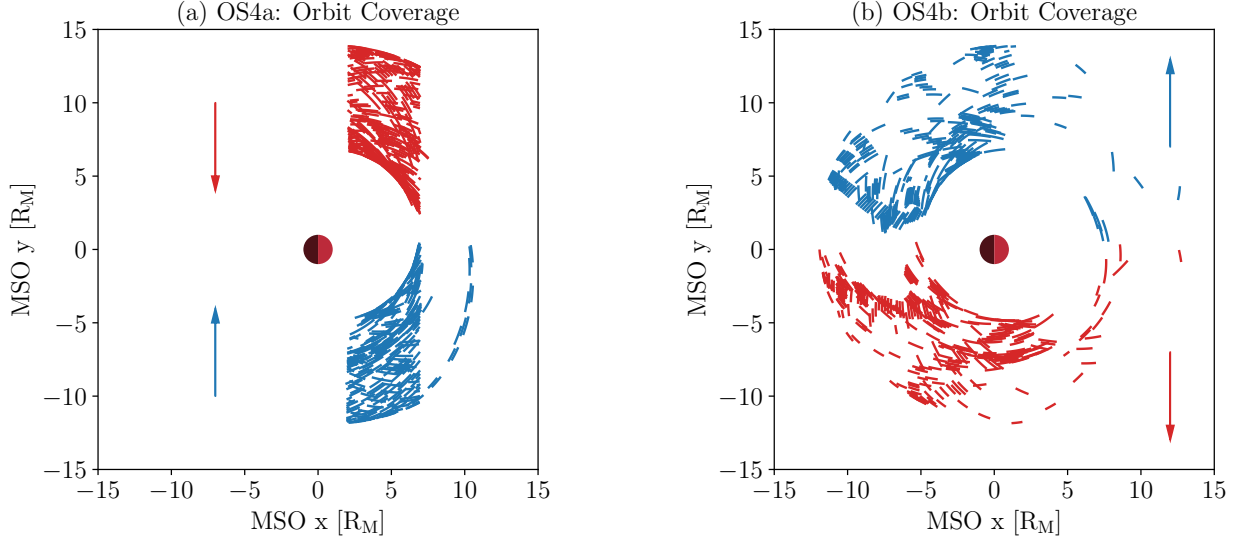


**Figure 1.** Location of EMM with pointing directions for a) EMUS OS4a foreground corona observations on the dayside b) EMUS OS4b interplanetary background observations. The arrows represent the look directions (towards Mars for OS4a and away from Mars for OS4b) with the red and blue arrows showing opposite look directions.

73 of the hot oxygen population was found to be hyper-thermal around  $\sim 1$  eV (Deighan et  
 74 al., 2015; Fox & Hać, 1997). Other photochemical processes and sputtering are thought to  
 75 operate in the Martian atmosphere, but are less important in the current epoch (Gröller et  
 76 al., 2014; Fox & Hać, 2018, 2014; Cravens et al., 2017; Leblanc et al., 2018, 2019; Zhang  
 77 et al., 2020; Krestyanikova & Shematovich, 2006; Shematovich, 2013; Jakosky et al., 1994;  
 78 Fox, 1993; Hodges Jr., 2000).

79 The oxygen atoms that are unable to escape from Mars are bound to the atmosphere  
 80 form a corona, which is an extended diffuse population of hot oxygen atoms that surrounds  
 81 the planet for several planetary radii. These oxygen atoms are either produced from the  
 82 less energetic dissociative recombination channels or through collisions with other atoms  
 83 and molecules. However, observing the oxygen corona has proven to be difficult due to its  
 84 tenuous nature (Deighan et al., 2015; Carveth et al., 2012). Previous studies have attempted  
 85 to observe it by using remote sensing measurements that focus on the relatively strong OI  
 86 130.4 nm triplet emission, which is a result of an electric dipole allowed transition ( $^3S \rightarrow$   
 87  $^3P$ ) of atomic oxygen. Solar resonant scattering is the main source for the OI 130.4 nm  
 88 emission line on Mars, which consists of three resonance triplet transitions of atomic oxygen  
 89 at 130.2, 130.5, and 130.6 nm respectively (Strickland et al., 1972, 1973). Spectroscopy for  
 90 the Investigation of the Characteristics of the Atmosphere of Mars (SPICAM) onboard Mars  
 91 Express observed the oxygen corona below  $\sim 500$  km (Montmessin et al., 2017) and ALICE  
 92 (Ultraviolet Imaging Spectrometer)/Rosetta observed the oxygen corona below  $\sim 1300$  km  
 93 during its flyby maneuver with a limited altitude sampling (Feldman et al., 2011). Despite  
 94 this, the expected brightness at altitudes above 700 km, where the hot oxygen population  
 95 dominates, is only between 1 to 10 Rayleighs, and had been very difficult to observe (Deighan  
 96 et al., 2015).

97 The Martian atomic oxygen exosphere is observed to have two components (Deighan  
 98 et al., 2015), as predicted by McElroy and Donahue (1972). This dual population of the  
 99 exosphere is seen when looking at the variation in altitude of the brightness of the 130.4  
 100 nm atomic oxygen resonant emission. This variation displays a clear two-slope altitude

101 dependence, with a rapid decrease in brightness above the exobase ( $\sim 1.06$  Mars radii or 200  
 102 km altitude), followed by a much slower decrease from typically 600 km altitude above the  
 103 surface of Mars (Deighan et al., 2015) (also see Figure 4a). The less energetic component in  
 104 the lower altitudes with a small-scale height is attributed to the thermal expansion of Mars’  
 105 atomic oxygen component above the Martian exobase, which is the thermal component  
 106 of the oxygen exosphere (Chaufray et al., 2015; Jain et al., 2015). The more energetic  
 107 component above 600 km is thought to be produced primarily by two processes occurring  
 108 in Mars’ upper atmosphere. These are the dissociative recombination of the most abundant  
 109 ion,  $O_2^+$ , in Mars’ ionosphere as mentioned above (Lee, Combi, Tenishev, Bougher, Deighan,  
 110 et al., 2015; Lee, Combi, Tenishev, Bougher, & Lillis, 2015) and the sputtering of the upper  
 111 atmosphere by precipitating pickup ions (Leblanc et al., 2015, 2018). These two processes are  
 112 thought to be the two main channels of Mars’ neutral atmospheric oxygen escape (Chaufray  
 113 et al., 2007, 2009; Yagi et al., 2012), although the role of electron impact excitation and  
 114 ionization of  $CO_2$  is also examined as an escape channel of neutral oxygen (Zhang et al.,  
 115 2020). Nagy and Cravens (1988) calculated the hot oxygen densities in the exosphere of  
 116 Mars, and compared those with the observed cold oxygen values from Viking database.

117 An indirect signature of Mars’ neutral oxygen escape was observed for the first time by  
 118 ALICE instrument on board Rosetta (Feldman et al., 2011) and was confirmed by the Imag-  
 119 ing Ultraviolet Spectrograph (IUVS) instrument on board Mars Atmosphere and Volatile  
 120 Evolution (MAVEN) spacecraft. The Phobos 2 plasma instruments were able to detect ener-  
 121 getic oxygen pickup ions near Mars associated with escaping hot oxygen atoms (Cravens et  
 122 al., 2002). Energetic oxygen pickup ions observed by SEP (Solar Energetic Particle), SWIA  
 123 (Solar Wind Ion Analyzer), and STATIC (Supra-Thermal and Thermal Ion Composition)  
 124 instruments on board MAVEN were used to infer exospheric oxygen densities and oxygen  
 125 escape rates (Rahmati et al., 2017, 2015, 2018; Ramstad et al., 2023).

126 In this study, we use 540 coronal emission profiles from  $\sim 1.28$  Mars years (consist-  
 127 ing of observations from Mars Year 36 and early Mars Year 37) of Emirates Mars Mission  
 128 (EMM)/Emirates Mars Ultraviolet Spectrometer (EMUS) data to understand and charac-  
 129 terize the variability in the OI 130.4 nm coronal emission with the Martian seasons and  
 130 solar forcing conditions. The following sections describe the instruments and data used, the  
 131 observations and discussion. Finally, the paper concludes by summarizing the observations  
 132 and describing the prospects for future work.

## 133 2 EMUS Cross Exospheric and Background Observations

134 In February 2021, the EMM spacecraft entered orbit around Mars and began to study  
 135 the atmosphere of Mars (Amiri et al., 2022; Almatroushi et al., 2021). EMM has a  $\sim 55$   
 136 hour period science orbit with a  $\sim 20,000$  km periapsis and  $\sim 43,000$  km apoapsis ( $6.9 R_M$   
 137  $\times 13.7 R_M$ ), and an orbital inclination of  $25^\circ$ . This unique orbit provides near-complete  
 138 geographic and diurnal coverage of Mars every  $\sim 10$  days (Amiri et al., 2022). EMM carries  
 139 the EMUS instrument (Holsclaw et al., 2021), which is an EUV/FUV spectrometer sensitive  
 140 to wavelengths between  $\sim 100$  nm and 170 nm. Light enters the spectrometer through a  
 141 narrow  $0.6^\circ \times 11^\circ$  slit. It is then focused by a spherical mirror onto a diffraction grating.  
 142 The grating splits the light into different “colors” (i.e. its spectral components). This  
 143 results in a two-dimensional image on a microchannel plate (MCP) detector with spectral  
 144 and spatial dimensions. Photon counts in each spatial and spectral bin is recorded in 50  
 145 second integrations for corona observations, called OS4 mode. Flight calibrations are carried  
 146 out using well-characterized stars, and also by observing the internal lamp to characterize  
 147 variations in spatial or temporal sensitivity. Holsclaw et al. (2021) describes in detail the  
 148 EMUS instrument, calibration, its science goals and the different observation strategies.

149 EMUS OS4 mode is designed to make coronal observations with a high signal to noise  
 150 ratio. This observation provides long exposure times for the inner, middle and outer Martian  
 151 exosphere. This mode is designed to occur when the spacecraft is charging in a near-inertial

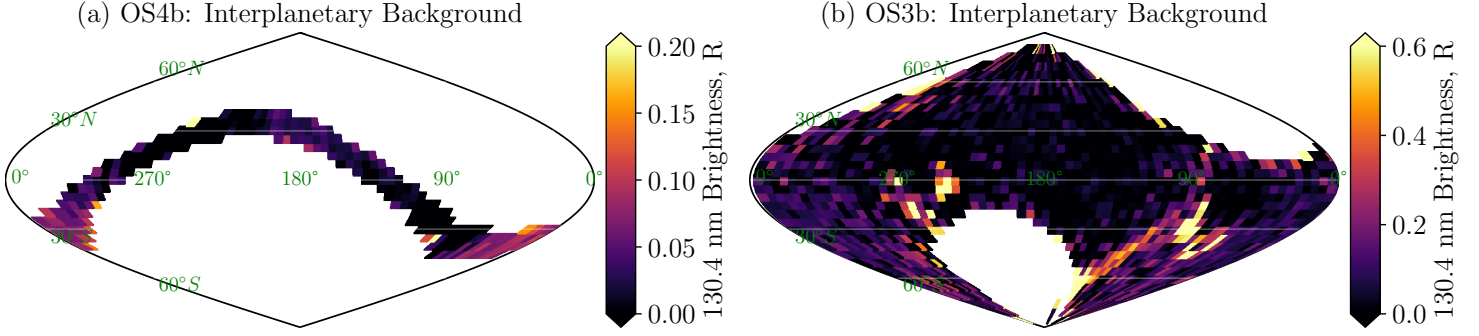


**Figure 2.** Sky maps of interplanetary background at 130.4 nm in ecliptic J2000 coordinates using a) EMUS OS4b background observations and b) EMUS OS3b background observations. The observations are binned in  $5^\circ$  ecliptic longitude by  $5^\circ$  ecliptic latitude bins. The bright patches correspond to the periods when the galactic plane was in the instrument viewing direction.

152 orientation (Holsclaw et al., 2021). There are two scenarios for this observation strat-  
 153 egy: exospheric or coronal observations (OS4a) and interplanetary background observations  
 154 (OS4b). OS4a is a cross-exosphere observation mode (or a limb scan that is made farther  
 155 away from the planet’s bright limb) by pointing the instrument across the EMM orbit and  
 156 along the Sun–Mars line. The instrument boresight vector is pointed in the plane of the  
 157 spacecraft orbit, perpendicular to both the Mars–Sun line and the orbit normal. EMUS is  
 158 observing lines of sight for tangent altitudes from 200 km to  $>17,000$  km ( $1.06 R_M$  to  $>6$   
 159  $R_M$ ) such that the boresight intersects the Mars–centered Solar Orbital (MSO) X-Z plane  
 160 (Holsclaw et al., 2021). The spectral resolution (or instrument slit position) is 1.8 nm, which  
 161 ensures adequate signal to noise while still spectrally separating the 130.4 nm oxygen signal  
 162 from neighboring lines. OS4b targets the interplanetary background and points in the same  
 163 direction (within  $2^\circ$ ; see Figure S1 of Supporting Information) of the OS4a that occurred  
 164 on the opposite side of the orbit, such that the EMUS boresight does not intersect the MSO  
 165 X-Z plane. The purpose of OS4b measurement is to distinguish the coronal foreground  
 166 emission from the interplanetary background emissions (Holsclaw et al., 2021).

167 The major backgrounds to the oxygen 130.4 nm emission are the 1) hydrogen Lyman  
 168 alpha wing background and the 2) interplanetary background. Hydrogen Lyman alpha (HI  
 169 121.6 nm) is by far the brightest emission line in EMUS data, and all other emissions are  
 170 sitting either on the shorter wavelength side or the longer wavelength side of this bright  
 171 emission feature. Hence, the spectral smearing of an atomic line is characterized by the  
 172 instrument Line Spread Function (LSF) (Jain et al., 2022; Chaffin et al., 2018; Deighan  
 173 et al., 2015). This background is subtracted by calculating the baseline fit based on the  
 174 shorter wavelength and longer wavelength sides of 130.4 nm core, that falls on the Lyman  
 175 alpha wing, but not on the 130.4 nm emission feature itself. More details of H Lyman alpha  
 176 wing subtraction from OI 130.4 nm emission are provided in the Supporting Information  
 177 (see Figure S4 of SI).

178 The interplanetary background is due to emissions that are unrelated to the oxygen  
 179 corona, but are emitted by the interplanetary sources such as dust, interstellar medium,  
 180 and diffuse emissions from the galactic plane. This background is subtracted by using the  
 181 OS4b mode of observations, which is designed to observe the interplanetary background  
 182 corresponding to each of the coronal (OS4a) observations. We find the nearest available  
 183 background observation (OS4b) corresponding to each of the foreground coronal observa-  
 184 tion (OS4a) to perform the subtraction. In addition to these two prominent backgrounds,  
 185 continuum emissions due to bright stars are also common. These appear as bright features

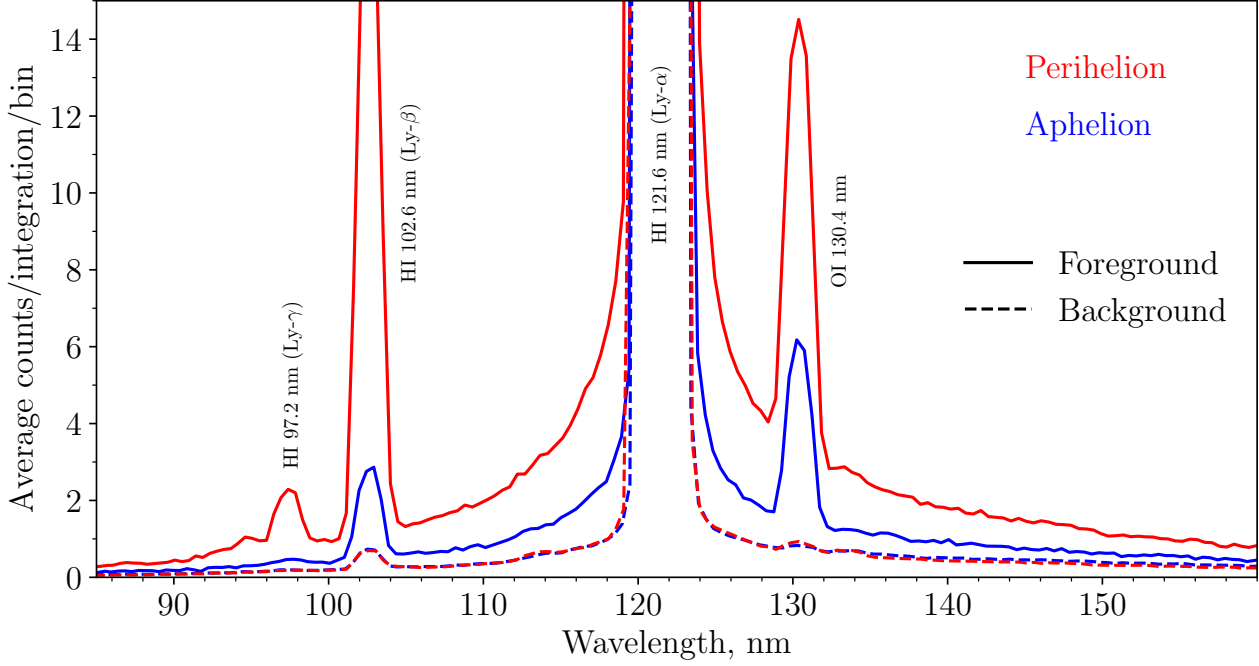


**Figure 3.** Examples of coronal (solid curve) and interplanetary background (dashed curve) spectra in average counts per integration per spatial bin observed by EMUS for aphelion and perihelion seasons. The tangent altitude range averaged for obtaining the foreground spectra is 2000 to 2500 km. The corresponding integration time for the foreground spectra is  $\sim 9$  minutes (11 integrations with a single integration time of 50 seconds). The integration time for the background spectra is  $\sim 57$  minutes (69 integrations with a single integration time of 50 seconds). For the examples shown above, the aphelion corona spectra is obtained on August 12, 2021, while the corresponding background spectra is obtained on August 11, 2021. The perihelion corona spectra is obtained on June 5, 2022, while the corresponding background spectra is obtained on June 8, 2022.

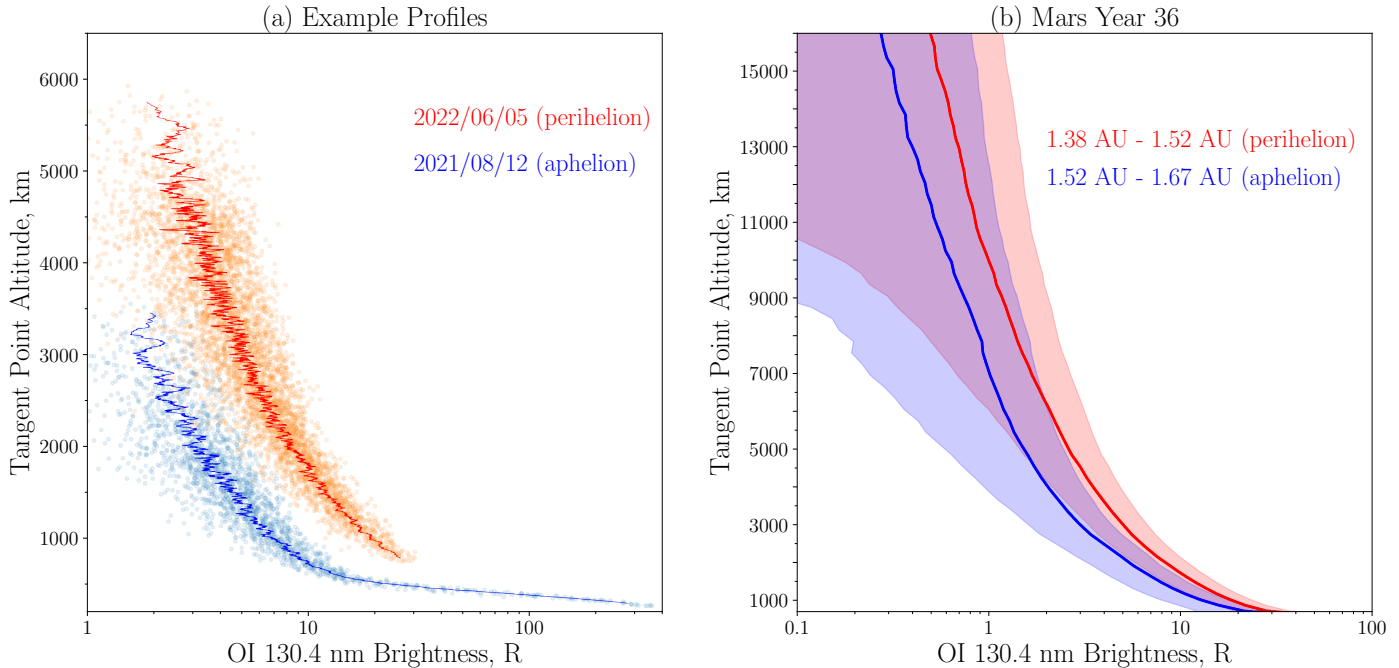


**Figure 4.** a) Example brightness vs. altitude profiles obtained using the same set of observations as in Figure 3 for aphelion (August 12, 2021) and perihelion (June 5, 2022) periods. The scattered points are individual samples (pixels) and the solid lines are the 20-samples rolling averages, b) averaged brightness vs. altitude profiles with  $1\sigma$  errorbars for MY 36 shown for two ranges of Sun–Mars distance, viz. perihelion (1.38–1.52 AU) and aphelion (1.52–1.67 AU) in red and blue respectively.

186 that contaminate certain pixels of the image. A star subtraction algorithm has been devel-  
 187 oped to remove this stellar contamination. This method works by identifying and removing  
 188 the contaminated pixels by looking at the higher wavelength (132.5 nm to 162 nm, avoiding  
 189 both OI 130.4 nm and the HI 121.6 nm ghost feature near 163 nm at the nominal grating  
 190 position) where we don’t expect any emissions from the Mars exosphere, while the stars are  
 191 still featured.

### 192 3 Altitude, Solar Zenith Angle and Seasonal Variability

193 Figures 1a and 1b show the orbit coverage in the Mars–centered Solar Orbital (MSO)  
 194 coordinate system. MSO +X is sunward from the center of the planet, +Y is duskward,  
 195 and the Z direction completes the right–handed system with +Z towards the north ecliptic  
 196 pole. Figure 1a shows the segments of orbits where cross-exospheric observations (OS4a)  
 197 were made on the dayside, while Figure 1b shows the segments of orbits where interplanetary  
 198 background observations (OS4b) were made by looking away from Mars. Additional  
 199 information on geographic coverage, sky coverage, coverage of tangent altitudes, solar zenith  
 200 angle, Sun–Mars distance, right ascension and declination are provided in the Supporting  
 201 Information (see Figures S1, S2, and S3 of SI).

202 Figure 2 shows the maps of interplanetary background at 130.4 nm wavelength. Figure  
 203 2a is made with the OS4b mode of observations, while Figure 2b is made with an observa-  
 204 tion mode of EMUS called OS3b. OS3b has more coverage on the sky, but are quick scans  
 205 (integration time of 0.7 seconds) designed mainly for hydrogen Lyman alpha observations

(Holsclaw et al., 2021). Both OS3b and OS4b are designed to observe the interplanetary background to exospheric observations (i.e., OS3a and OS4a respectively). The major difference is their sky coverage and integration time. OS3b slew across  $100^\circ$  in an asterisk pattern centered on the disk (0.7 seconds integrations), while OS4b scans a comparably smaller sky, but providing long exposure times (50 seconds integrations). These background observations, especially OS4b, allows for the oxygen from the Martian exosphere to be distinguished from the interplanetary emission contributions (Holsclaw et al., 2021). The images show the presence of two bright regions on the sky, mainly due to the presence of galactic plane in the line of sight during those observation periods.

Figure 3 shows examples of EMUS OS4 spectra during aphelion period (in blue) and perihelion period (in red). The solid curves show the coronal spectra (OS4a), while dashed curves show the interplanetary background spectra (OS4b). The aphelion corona spectra shown is obtained on August 12, 2021, while the corresponding background spectra is obtained on August 11, 2021. The perihelion corona spectra shown is obtained on June 5, 2022, while the corresponding background spectra is obtained on June 8, 2022. The perihelion spectra have generally higher intensities as compared to the aphelion spectra as expected. A tangent altitude range of 2000 to 2500 km is co-added for obtaining the foreground spectra. The corresponding integration time for the foreground spectra is  $\sim 9$  minutes (11 integrations with a single integration time of 50 seconds). The integration time for the background spectra is  $\sim 57$  minutes (69 integrations with a single integration time of 50 seconds). It may be noted that the background spectra during both periods are nearly of the same intensities. The lack of difference between the background spectra at perihelion and aphelion confirms that the Martian oxygen exospheric contribution is negligible and this measurement is a good estimator of the interplanetary 130.4 nm brightness. The difference in brightness enhancement for OI 130.4 nm and HI 102.6 nm emissions between the two seasons indicates their different emission sources.

Figure 4a shows examples of OI 130.4 nm brightness vs. altitude profiles obtained using the same set of observations after background subtraction (both H Lyman alpha wing background and the interplanetary background). These observations are representative of several observations done using a similar strategy. The example days chosen for aphelion and perihelion are the same as in the spectra (Figure 3). A comparison between an averaged oxygen corona profile from MAVEN/IUVS (Figure 3c of Deighan et al. (2015)) and an EMUS OS4 profile for a comparable season and solar activity period in 2022 is shown in Figure S5 of the Supporting Information. We can see that the profiles are matching between the two observations. We have also calculated the column density profiles for the average EMUS OS4 oxygen brightness profiles shown in Figure 4a. The aphelion column densities vary between  $\sim 8.26e7 \text{ cm}^{-2}$  to  $4.65e5 \text{ cm}^{-2}$  for an altitude range of  $\sim 297 \text{ km}$  to  $3453 \text{ km}$ . The details of column density estimation based on a nominal  $g$ -factor (fluorescence efficiency factor) that is scaled for Sun–Mars distance is given in Supporting Information (Figure S6). Figure 4b shows the average brightness vs. altitude profiles for two ranges of Sun–Mars distance (1.38–1.52 AU and 1.52–1.67 AU). The errorbar (one standard deviation of the population) is shown as the color fill around the solid curves. Both Figures 4a and 4b clearly depict the brightness variation that is due to changing altitude as well as the changing Sun–Mars distance. It can be noted that higher brightness is observed during perihelion as compared to the aphelion.

Figure 5 shows the binned images of OI 130.4 nm brightness variation with altitude and as a function of Solar Zenith Angle (SZA) and Martian season ( $L_s$ ). Figure 5a shows the variation of brightness as a function of altitude and SZA. Altitude and SZA are those of the tangent point of the line of sight. The altitude bin size is 500 km and the SZA bin size is 5 degrees. The SZA variation during this period is 0 to  $\sim 60$  degrees, making them on the dayside close to noon. Higher brightness is observed near noon as compared to higher SZAs. Figure 5b shows the brightness variation as a function of altitude and Martian season ( $L_s$ ). Here also the altitude bin size is 500 km, and the  $L_s$  bin size is 10 degrees. The contours of

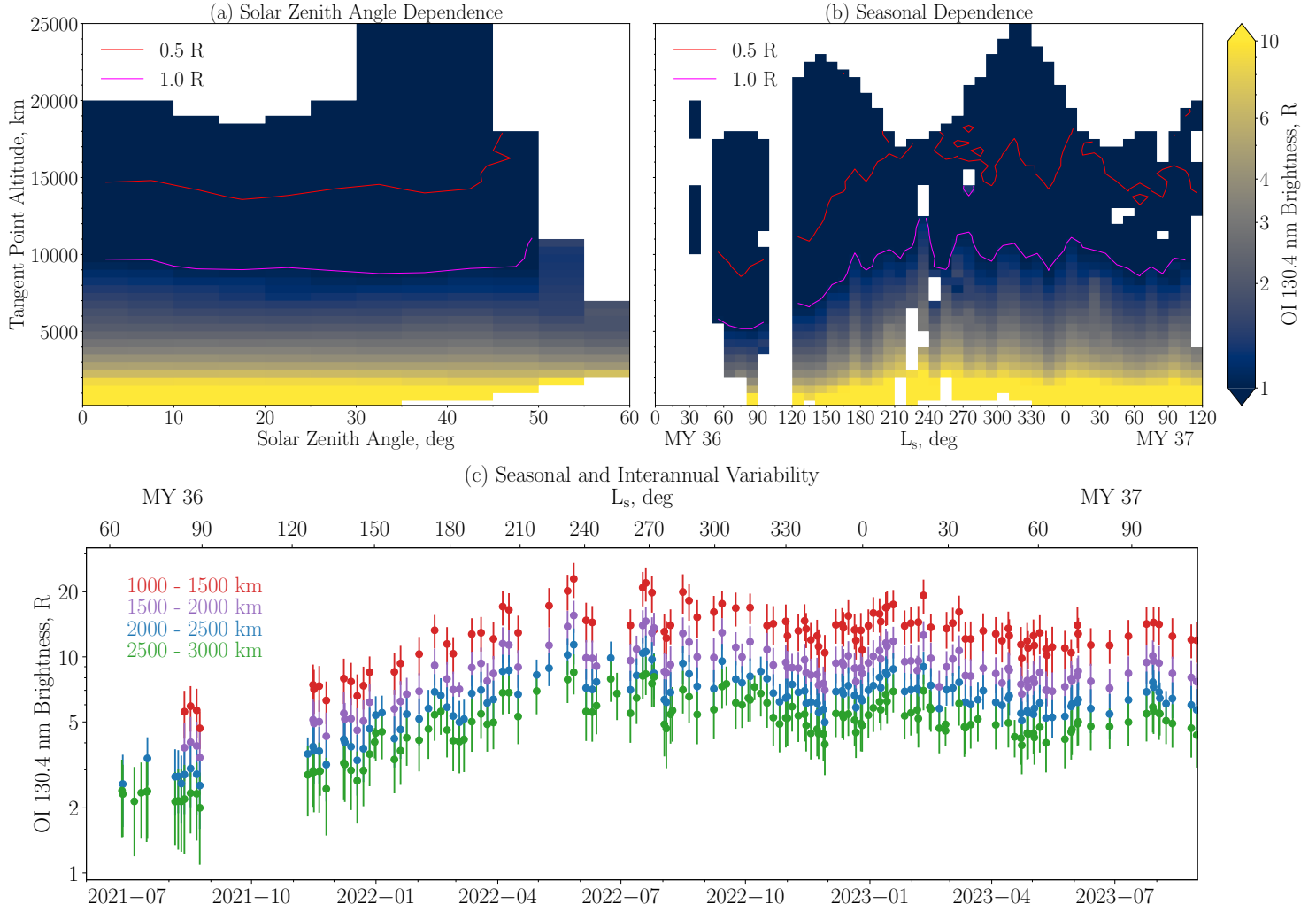


**Figure 5.** Binned images of OI 130.4 nm brightness as a function of a) Solar Zenith Angle (SZA) and altitude and b) Martian Solar Longitude ( $L_s$ ) and altitude. The 0.5 R (red) and 1.0 R (magenta) contours are also shown. Panel c) shows the timeline of O corona brightness for four different altitude ranges from 1000 to 3000 km. Aphelion is when  $L_s$  is  $71^\circ$  and perihelion is when  $L_s$  is  $251^\circ$ . Note that the brightness scale is logarithmic. Interannual variability during the aphelion periods of MY 36 and MY 37 can also be noted in Figures 5b and 5c. The data gap between  $L_s$   $100^\circ$  and  $120^\circ$  in MY 36 is due to the absence of data collection during solar conjunction period.

259 0.5 R and 1.0 R are also shown for reference on both images. Figure 5c shows the timeline  
 260 of brightness variation at four different altitude ranges from 1000 to 3000 km, each averaged  
 261 over a 500 km altitude bin size. It can be seen that the oxygen corona is brighter during the  
 262 perihelion season as compared to aphelion season at all the tangent altitudes shown here.  
 263 Also, the interannual variability from MY 36 to MY 37 aphelion periods can be noted. The  
 264 aphelion of MY 37 is brighter as compared to the aphelion of MY 36, primarily due to the  
 265 rising Solar Cycle 25.

#### 266 4 Variability with Solar Irradiance

267 Figure 6 shows the temporal variability of O corona brightness, solar irradiance and  
 268 the backgrounds to coronal OI 130.4 nm emission. Figure 6a shows the EMUS observed  
 269 130.4 nm emission brightness at a tangent point altitude of 2000 km to 2500 km. This range  
 270 was chosen because it is one of the altitude ranges with the highest OS4a altitude sampling  
 271 coverage and a good signal-to-noise ratio. Additionally, this altitude is well above the region  
 272 of cold oxygen. The average and one standard deviation of the population as error bar is  
 273 also shown. The range of values observed is shown as the scatter points. We can notice  
 274 that the oxygen intensity peaks around perihelion ( $L_s \sim 251^\circ$ ). The brightness ratio between  
 275 perihelion and aphelion is approximately 4.5. Figure 6b shows the temporal variability of  
 276 solar 0–91 nm ionizing EUV irradiance and solar 130.4 nm irradiance from MAVEN/EUVM  
 277 (Eparvier et al., 2015). EUVM has three calibrated photometers designed to measure the  
 278 variability of the solar soft x-rays and EUV irradiance at Mars in three bands. In this  
 279 study, we use the EUVM Level 3 modeled data, which is a combination of observations at  
 280 Mars and time-interpolated observations at Earth using the spectral irradiance variability  
 281 model called the Flare Irradiance Spectral Model-Mars (FISM-M) (Thiemann et al., 2017).  
 282 The gap in the data from February 23, 2022 to April 21, 2022 is due to the absence of  
 283 MAVEN/EUVM data during that period (since MAVEN was in safe-mode). Figure 6c  
 284 shows the variation of hydrogen Lyman alpha wing under OI 130.4 nm. This background is  
 285 subtracted from the original spectra to get the oxygen brightness values (see Figure S4 of  
 286 Supporting Information). Figure 6d shows the interplanetary background at 130.4 nm using  
 287 the OS4b mode of observations. An error bar of one standard deviation of the population  
 288 is also shown. The interplanetary (sky) background at 130.4 nm roughly varies around  $\sim$   
 289 0.1 R. The solar irradiance is significantly increased from December 2022 onwards, which is  
 290 also reflected in the oxygen corona with a significant brightness enhancement (Figure 6).

291 Figure 7 shows the same parameters normalized for Sun–Mars distance. The normal-  
 292 ization is done to differentiate the variability in exospheric emission intensities and solar  
 293 irradiance measured at Mars that varies with both Sun–Mars distance and solar activity  
 294 progression. Figure 7a shows the O corona brightness normalized by  $[1/r^4]$ , where  $r$  is the  
 295 Sun–Mars distance. The normalization by  $[1/r^4]$  is done to account both the variation in  
 296 ionizing radiation (which affects the production of hot O atoms), as well as the variation  
 297 in fluorescence scattering (i.e., illumination conditions) with the changing Sun–Mars dis-  
 298 tance, with both factors contributing  $[1/r^2]$  each (Deighan et al., 2019). Figure 7b shows  
 299 the solar irradiance normalized by a factor  $[1/r^2]$ . This is done to account the variation in  
 300 solar irradiance measured at Mars with changing Sun–Mars distance. Figure 7c shows the  
 301 H Lyman alpha wing under OI 130.4 nm also normalized by  $[1/r^2]$ . Interestingly, we can  
 302 notice that the seasonal variation in hydrogen Lyman alpha wing intensities is still present  
 303 in the normalized plot, with the peak intensity during southern summer solstice ( $L_s \sim 270^\circ$ ).  
 304 Whereas, the normalized O corona intensity follows solar irradiance variation without any  
 305 perihelion peak, and the increase in oxygen signal over time must be due to some combina-  
 306 tion of higher solar activity (which is clear), but also possibly in the source of hot O atoms,  
 307 either due to electron temperatures (which mediate the rate of dissociative recombination),  
 308 ion temperatures (which affect the distribution of initial hot O atom energies following the  
 309 recombination reaction), or neutral density profiles (since collision with those neutrals affect  
 310 the energy distribution of exospheric O atoms). We have also calculated the ratio of coronal

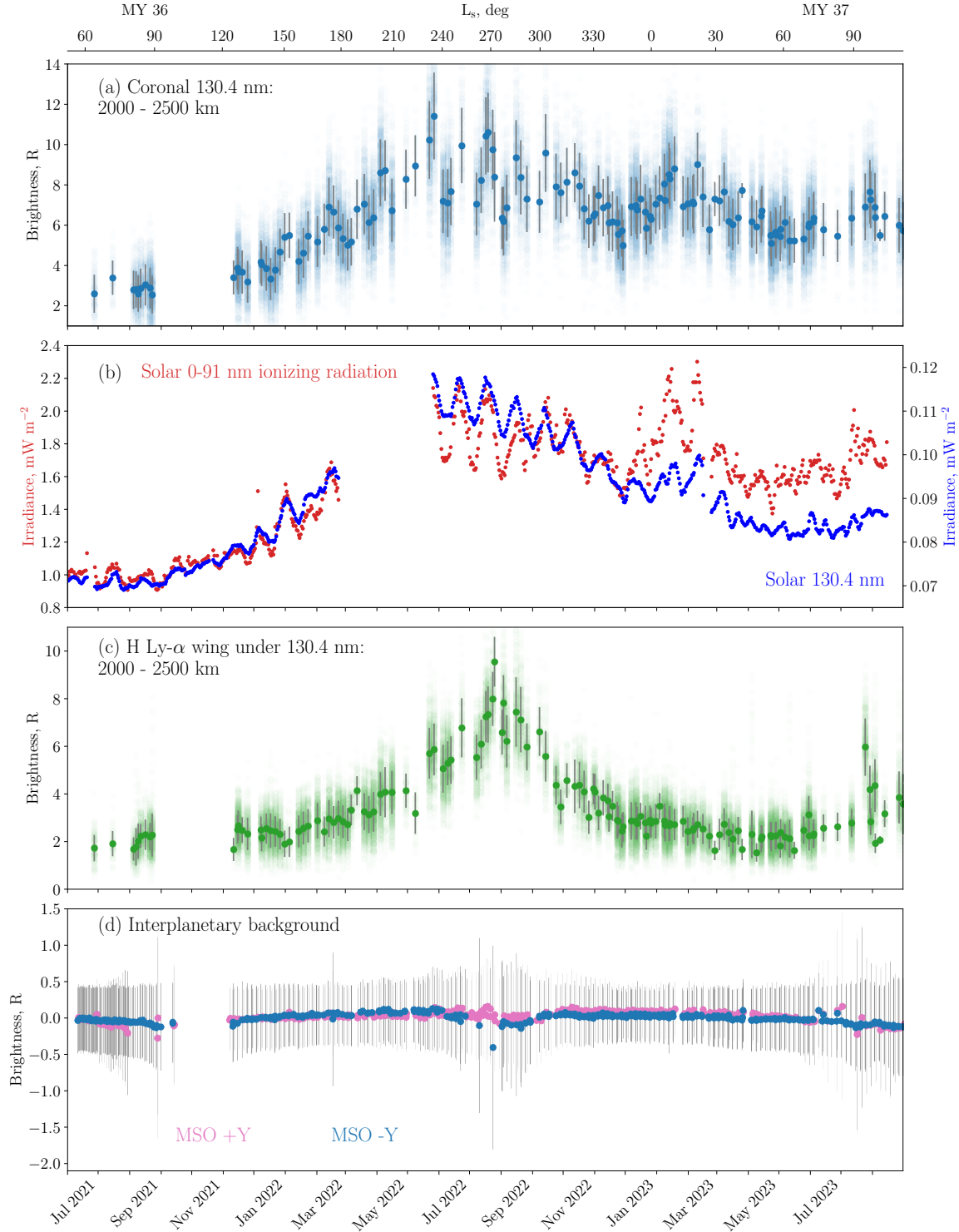


**Figure 6.** Temporal variability of a) OI 130.4 nm coronal brightness for an altitude range of 2000 to 2500 km, b) solar EUV 0-91 nm ionizing irradiance and solar 130.4 nm emissions at Mars, c) hydrogen Lyman alpha wing under EMUS OI 130.4 nm for the altitude range of 2000 to 2500 km, and d) interplanetary background at 130.4 nm, with  $1\sigma$  errorbars. The gap in EMUS data between  $L_s$  99 and 123 in MY 36 is due to the absence of EMM data collection during solar conjunction period. The gap in EUVM data between  $L_s$  179 and 212 in MY 36 is due to MAVEN in safe-mode.

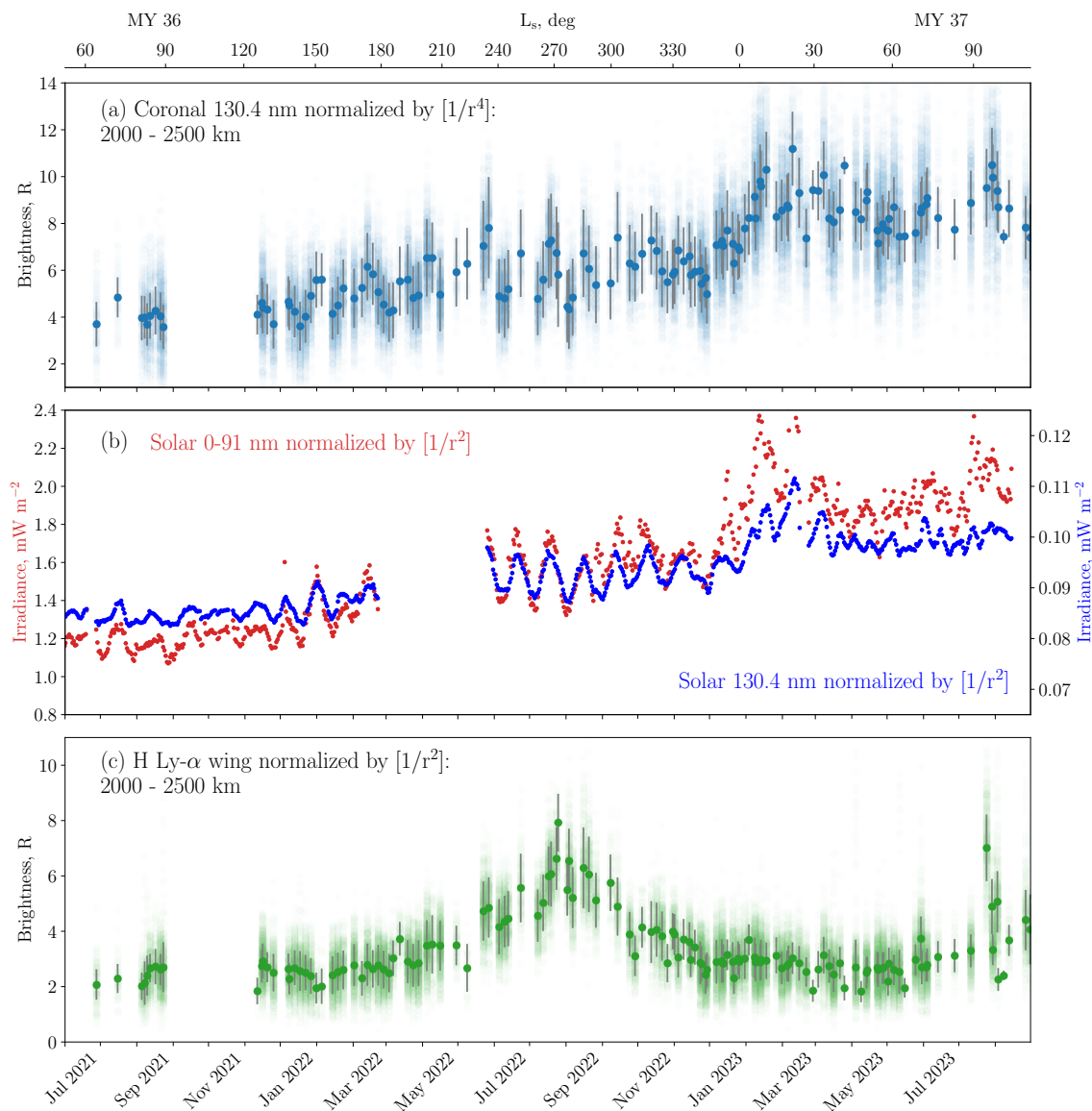


**Figure 7.** Temporal variability of coronal brightness and solar irradiance after normalizing for Sun–Mars distance. a) OI 130.4 nm coronal brightness normalized by  $1/r^4$ , where  $r$  is the Sun–Mars distance, b) solar irradiances at Mars normalized by  $1/r^2$ , and c) hydrogen Lyman alpha wing under OI 130.4 nm normalized by  $1/r^2$ . The gap in EMUS data between  $L_s$  99 and 123 in MY 36 is due to the absence of EMM data collection during solar conjunction period. The gap in EUVM data between  $L_s$  179 and 212 in MY 36 is due to MAVEN in safe-mode.

311 oxygen 130.4 nm brightness and solar irradiances (Figure S7 of the Supporting Information).  
 312 The ratio increases for the individual irradiances (i.e., solar 130.4 nm and 0–91 nm) but is  
 313 nearly constant for the product between the two. This implies a correlation between the  
 314 coronal brightness and the product of illuminating and photoionizing solar irradiances. We  
 315 will explore this further with the correlation analysis described in the next section.

#### 316 4.1 Coronal Correlation with Solar Irradiance

317 Figures 8a and 8b show the correlation between coronal 130.4 nm brightness and solar  
 318 irradiances. Linear regression is used to fit the data points. Figure 8a shows the variation of  
 319 coronal OI 130.4 nm as a function of solar ionizing irradiance (0–91 nm). Figure 8b shows  
 320 the variation of coronal 130.4 nm as a function of solar 130.4 nm irradiance. Both plots  
 321 indicate that the coronal oxygen brightness has a near linear relationship with the solar  
 322 irradiance. Figure 8c is the correlation between coronal oxygen brightness and the product  
 323 of solar ionizing irradiance and solar 130.4 nm emissions. The data points are having the  
 324 highest goodness of fit ( $R^2 = 0.92$ ) and correlation coefficient ( $R = 0.96$ ) with the product  
 325 as compared to the individual irradiances. Coronal oxygen brightness is expected to vary  
 326 positively with both solar EUV as well as the solar oxygen emission at 130.4 nm. The first  
 327 because EUV produces the ions necessary for dissociative recombination and the second  
 328 because solar 130.4 nm is the source of illumination for the oxygen resonance line scattering  
 329 in the corona that EMUS observes. The current analysis suggests that variations in the  
 330 brightness of the hot coronal oxygen population at Mars are strongly related with changes  
 331 in ionizing solar EUV flux (correlation coefficient,  $R = 0.92$ ) than the illuminating solar 130.4  
 332 nm line (correlation coefficient,  $R = 0.86$ ). The higher correlation of coronal brightness with  
 333 EUV flux is consistent with an expected ionospheric photochemical source (Deighan et al.,  
 334 2015).

335 For comparison, we are also showing the correlation between solar photoionizing irradi-  
 336 ance and the product of coronal oxygen 130.4 nm brightness and solar 130.4 nm irradiance  
 337 (Figure S8a), as well as the correlation between solar 130.4 nm and the product of coronal  
 338 oxygen 130.4 nm brightness and solar photoionizing irradiance (Figure S8b) in the Sup-  
 339 porting Information. These correlation graphs (Figure S8) are similar to Figures 8a and  
 340 8b respectively. It may also be noted that photoelectron impact excitation source of OI  
 341 130.4 nm in the corona is negligible (Chaufray et al., 2015, 2009). Additionally, since this  
 342 emission is optically thick (especially at low altitudes), the scale height of the brightness is  
 343 influenced by both density and temperature (Chaufray et al., 2015). But at altitudes 2000–  
 344 2500 km, the electron impact is expected to be negligible (it is less valid at lower altitudes)  
 345 and the oxygen emission is optically thin. Even the planet shine (backscatter photons from  
 346 the optically thick region at lower altitudes) is expected to be small (Chaufray et al., 2016).  
 347 Therefore, an increase in coronal brightness imply an increase in coronal density.

#### 348 4.2 Solar Rotation Effect in the Corona

349 The left side panels in Figure 9 show the time series of MAVEN EUVM data and EMM  
 350 EMUS data normalized for Sun–Mars distance. The EMUS data shown is for a tangent  
 351 altitude range of 2500 to 3000 km. The 81-days rolling average of the signal as well as the  
 352 residual after subtracting the rolling average is also shown. The right side panels of Figure 9  
 353 show the Lomb-Scargle periodograms obtained using the residual EUVM and EMUS signals.  
 354 The moving average is subtracted in order to remove the long term periodicities and their  
 355 sub-harmonics in the data, which is caused by Sun–Mars distance/seasonal variation, and  
 356 inter-annual variations.

357 The prominent short term periodicity in both the datasets is quasi-27-days due to  
 358 solar rotation. The peak corresponding to solar rotation is above the 95% confidence level.  
 359 Other prominent periodicities adjacent to the quasi-27-days are a result of the active regions  
 360 contributing to the solar rotation variability being located at different latitudes. Also, solar

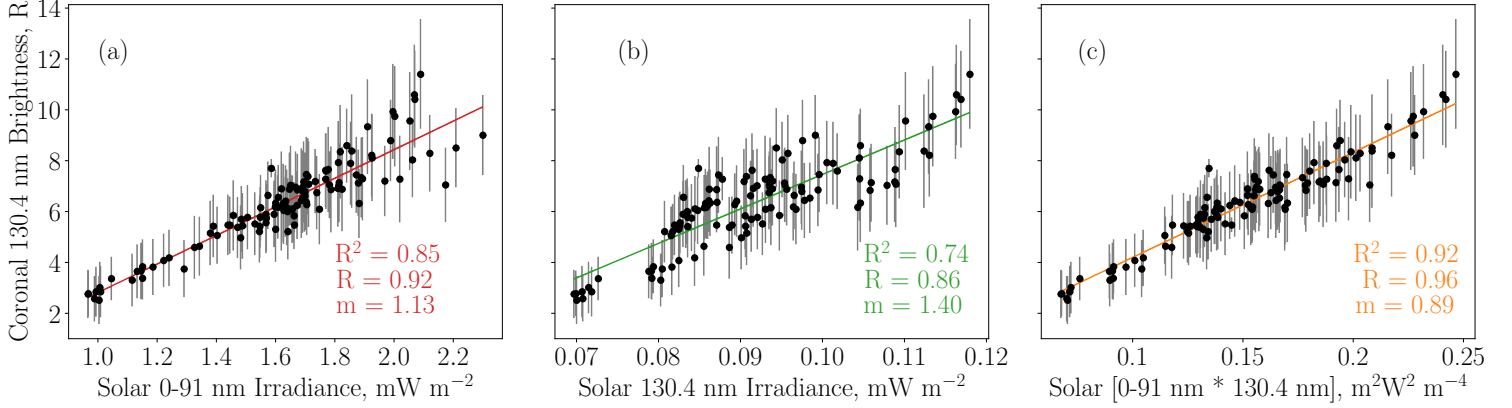


**Figure 8.** a) Correlation between solar EUV 0–91 nm ionizing irradiance and coronal oxygen 130.4 nm brightness, b) correlation between solar 130.4 nm and coronal oxygen 130.4 nm, and c) correlation between the product of solar EUV ionizing and solar 130.4 nm irradiances, and coronal oxygen 130.4 nm brightness. The coronal brightness is for an altitude range of 2000 – 2500 km. The symbol  $m$  is the normalized slope (normalized by the maximum value of brightness and irradiances) of the fit,  $R$  is the correlation coefficient, and  $R^2$  is the goodness of fit.

361 rotation is differential with the equator rotating faster (taking only about 24 days) than the  
 362 poles (which rotate once in more than 30 days) (Javaraiah, 2011). The periodograms for  
 363 three other example altitude ranges (1000–1500 km in gray, 1500–2000 km in light purple,  
 364 2000–2500 km in light blue) are also shown in Figure 9d for comparison. We can notice that  
 365 the normalized Lomb-Scargle power for the main periodicity peak around quasi-27-days is  
 366 similar across these different altitude ranges. Hence, the effect of solar rotation must be  
 367 consistent at these varying altitudes.

## 368 5 Conclusions and Future Prospects

369 EMM/EMUS oxygen corona observations using the long exposure time scans reveal for  
 370 the first time the dependence of brightness on Sun–Mars distance and solar forcing. EMUS  
 371 OS4 data is highly sensitive to the OI 130.4 nm emission from the Martian exosphere and we  
 372 have shown O corona observations upto an altitude of  $>6 R_M$ . The background observations  
 373 enable us to subtract the interplanetary contributions to the foreground data. In addition  
 374 to the strong Sun–Mars distance, solar zenith angle and solar EUV flux dependence, the  
 375 O corona also shows a short term variability due to solar rotation. The prominent short  
 376 term periodicity in both EUVM and EMUS data is the quasi-27-days solar rotation period.  
 377 Correlation of the oxygen corona brightness with EUVM solar irradiance measurements  
 378 suggests a relationship between coronal density and solar photoionizing flux. This supports  
 379 the expectation that dissociative recombination in the ionosphere is the main source of hot  
 380 oxygen on Mars (although sputtering also increases with photoionizing flux, it is dwarfed  
 381 by the dissociative recombination).

382 The effects of episodic events such as solar flares (Lee et al., 2018) and dust storms (Lee  
 383 et al., 2020; Huang et al., 2022), as well as the influence of solar wind on oxygen corona  
 384 (Ramstad et al., 2023; Shematovich, 2021) needs further investigation. The effect of Martian  
 385 crustal magnetic fields on the oxygen corona, if any, is also in need of investigation, although  
 386 we do not expect to see any crustal field effects at these very high altitudes, since the corona  
 387 is expected to become more uniform as the spatial variations become more globally averaged.  
 388 However, the structure of the inner oxygen corona is expected to retain the strongest imprint

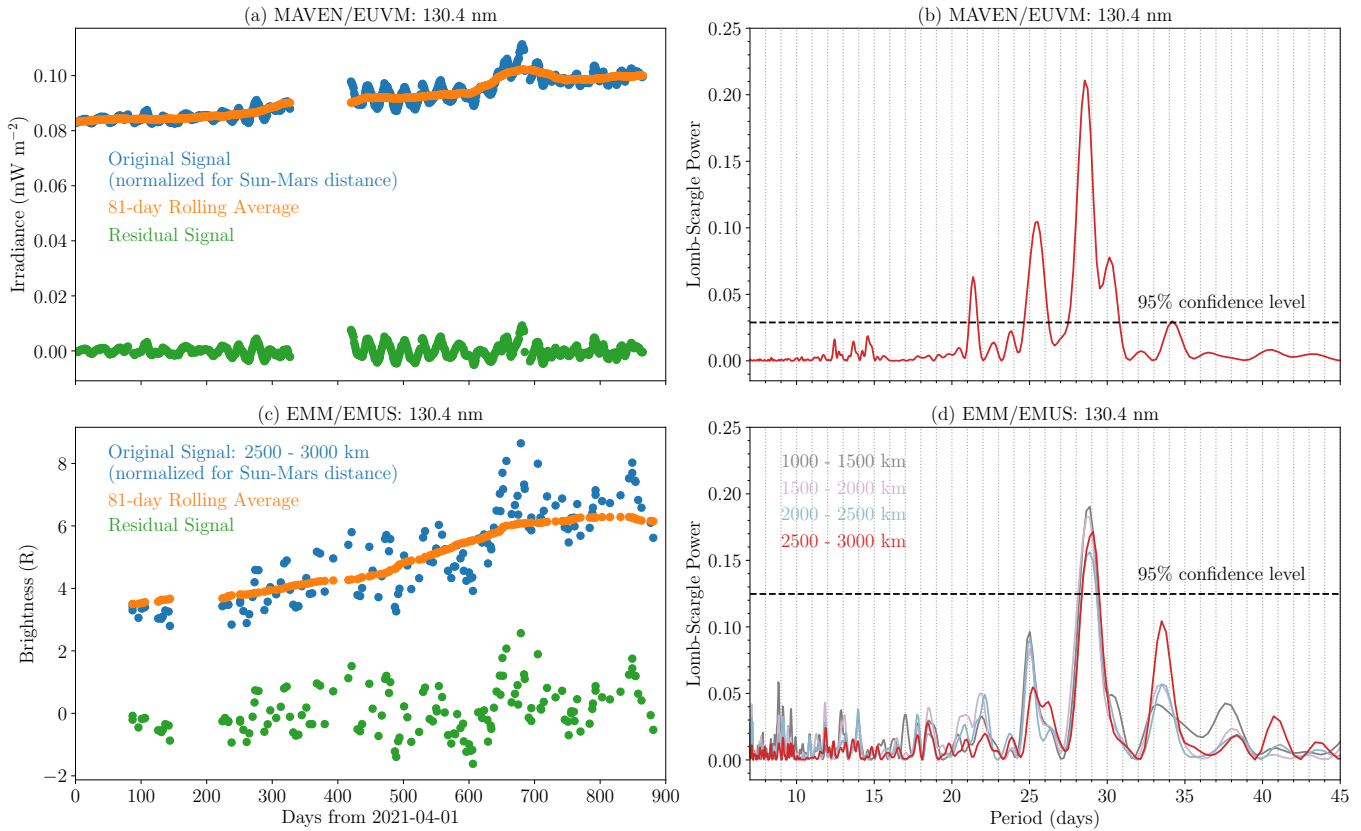


**Figure 9.** a) Time series of normalized EUVM 130.4 nm solar irradiance (blue), moving average corresponding to three solar rotations (orange), and the residual signal after subtracting the moving average (green). b) Lomb-Scargle periodogram for the residual EUVM signal (red). c) Time series of normalized EMUS OI 130.4 nm daily averaged coronal brightness for an altitude range of 2500 to 3000 km (blue), moving average corresponding to three solar rotations (orange), and the residual signal after subtracting the moving average (green). d) Lomb-Scargle periodogram for the residual EMUS signal (red). The 95% confidence level for both periodograms are also shown (black dashed lines). The other periodograms in the panel (d) are for three other altitude ranges in Figure 5c and are shown for comparison (1000–1500 km in gray, 1500–2000 km in light purple, 2000–2500 km in light blue).

389 of any spatial variations in the photochemical source such as due to crustal fields around the  
 390 globe (Deighan et al., 2022). The global imaging of the 3D distribution of the inner oxygen  
 391 corona from EMUS will be presented in a different paper (Deighan et al., 2022; Holsclaw et  
 392 al., 2021).

393 The brightness observation is the first step to the derivation of exospheric density and  
 394 temperature (Chaufray et al., 2009). The next step would be to calculate, using modeling,  
 395 the escape rate of oxygen atoms that are escaping via non-thermal photochemical mech-  
 396 anisms. Escape flux of hot oxygen during different seasons can be calculated using these  
 397 EMUS derived input parameters as well as the near-simultaneous in-situ neutral, ion and  
 398 electron measurements from MAVEN (Lillis et al., 2017; Chirakkil et al., 2022; Cravens et  
 399 al., 2017). The observed brightness is also a constraint on models of hot oxygen that can  
 400 calculate not only the escape rate but also the hot oxygen density and effective temperature  
 401 (Leblanc et al., 2017; Qin et al., 2024).

## 402 Open Research Section

### 403 Data Availability Statement

404 The EMM/EMUS l2a data we analyze here are available at the EMM Science Data  
 405 Center (SDC, <https://sdc.emiratesmarsmission.ae/>). This location is designated as the  
 406 primary repository for all data products produced by the EMM team and is designated as  
 407 long-term repository as required by the UAE Space Agency. The data available ([https://](https://sdc.emiratesmarsmission.ae/data)  
 408 [sdc.emiratesmarsmission.ae/data](https://sdc.emiratesmarsmission.ae/data)) include ancillary spacecraft data, instrument telemet-  
 409 ry, Level 1 (raw instrument data) to Level 3 (derived science products), quicklook prod-  
 410 ucts, and data users guides (<https://sdc.emiratesmarsmission.ae/documentation>) to  
 411 assist in the analysis of the data. Following the creation of a free login, all EMM data  
 412 are searchable via parameters such as product file name, solar longitude, acquisition time,  
 413 sub-spacecraft latitude and longitude, instrument, data product level, etc. EMUS data and  
 414 users guides are available at: <https://sdc.emiratesmarsmission.ae/data/emus>. The  
 415 MAVEN EUVM L3 data are publicly available at the NASA Planetary Data System through  
 416 <https://pds-ppi.igpp.ucla.edu/data/maven-euv-modelled>.

### 417 Acknowledgments

418 Funding for development of the EMM mission is provided by the UAE government, and  
 419 to co-authors outside of the UAE by MBRSC. KC and SR are supported by the grant  
 420 8474000332-KU-CU-LASP Space Sci. ET, PC, FE, and SC are supported by NASA through  
 421 the MAVEN project.

### 422 References

- 423 Almatroushi, H., AlMazmi, H., AlMheiri, N., AlShamsi, M., AlTunaiji, E., Badri, K., . . .  
 424 Young, R. M. B. (2021, December). Emirates Mars Mission Characterization of  
 425 Mars Atmosphere Dynamics and Processes. *Space Science Reviews*, *217*(8), 89. doi:  
 426 10.1007/s11214-021-00851-6
- 427 Amiri, H. E. S., Brain, D., Sharaf, O., Withnell, P., McGrath, M., Alloghani, M., . . . Yousuf,  
 428 M. (2022, February). The Emirates Mars Mission. *Space Science Reviews*, *218*(1), 4.  
 429 doi: 10.1007/s11214-021-00868-x
- 430 Barth, C. A., Hord, C. W., Pearce, J. B., Kelly, K. K., Anderson, G. P., & Stew-  
 431 art, A. I. (1971). Mariner 6 and 7 Ultraviolet Spectrometer Experiment: Up-  
 432 per atmosphere data. *Journal of Geophysical Research (1896-1977)*, *76*(10), 2213-  
 433 2227. Retrieved from [https://agupubs.onlinelibrary.wiley.com/doi/abs/10](https://agupubs.onlinelibrary.wiley.com/doi/abs/10.1029/JA076i010p02213)  
 434 [.1029/JA076i010p02213](https://doi.org/10.1029/JA076i010p02213) doi: <https://doi.org/10.1029/JA076i010p02213>
- 435 Carveth, C., Clarke, J., Chaufray, J., & Bertaux, J. (2012, October). Analysis Of HST  
 436 Spatial Profiles Of Oxygen Airglow From Mars. In *Aas/division for planetary sciences*

- 437 *meeting abstracts #44* (Vol. 44, p. 214.03).
- 438 Chaffin, M. S., Chaufray, J. Y., Deighan, J., Schneider, N. M., Mayyasi, M., Clarke,  
439 J. T., ... Jakosky, B. M. (2018). Mars H Escape Rates Derived From  
440 MAVEN/IUVS Lyman Alpha Brightness Measurements and Their Dependence on  
441 Model Assumptions. *Journal of Geophysical Research: Planets*, 123(8), 2192-  
442 2210. Retrieved from [https://agupubs.onlinelibrary.wiley.com/doi/abs/10](https://agupubs.onlinelibrary.wiley.com/doi/abs/10.1029/2018JE005574)  
443 [.1029/2018JE005574](https://agupubs.onlinelibrary.wiley.com/doi/abs/10.1029/2018JE005574) doi: <https://doi.org/10.1029/2018JE005574>
- 444 Chaufray, J. Y., Deighan, J., Chaffin, M. S., Schneider, N. M., McClintock, W. E., Stew-  
445 art, A. I. F., ... Jakosky, B. M. (2015). Study of the Martian cold oxygen corona  
446 from the O I 130.4 nm by IUVS/MAVEN. *Geophysical Research Letters*, 42(21),  
447 9031-9039. Retrieved from [https://agupubs.onlinelibrary.wiley.com/doi/abs/](https://agupubs.onlinelibrary.wiley.com/doi/abs/10.1002/2015GL065341)  
448 [10.1002/2015GL065341](https://agupubs.onlinelibrary.wiley.com/doi/abs/10.1002/2015GL065341) doi: <https://doi.org/10.1002/2015GL065341>
- 449 Chaufray, J.-Y., Deighan, J., Stewart, A. I. F., Schneider, N., Clarke, J., Leblanc, F.,  
450 & Jakosky, B. (2016). Effect of the planet shine on the corona: Application to  
451 the Martian hot oxygen. *Journal of Geophysical Research: Space Physics*, 121(11),  
452 11,413-11,421. Retrieved from [https://agupubs.onlinelibrary.wiley.com/doi/](https://agupubs.onlinelibrary.wiley.com/doi/abs/10.1002/2016JA023273)  
453 [abs/10.1002/2016JA023273](https://agupubs.onlinelibrary.wiley.com/doi/abs/10.1002/2016JA023273) doi: <https://doi.org/10.1002/2016JA023273>
- 454 Chaufray, J. Y., Leblanc, F., Quémerais, E., & Bertaux, J. L. (2009). Martian oxygen  
455 density at the exobase deduced from O I 130.4-nm observations by Spectroscopy for  
456 the Investigation of the Characteristics of the Atmosphere of Mars on Mars Express.  
457 *Journal of Geophysical Research: Planets*, 114(E2). Retrieved from [https://agupubs](https://agupubs.onlinelibrary.wiley.com/doi/abs/10.1029/2008JE003130)  
458 [.onlinelibrary.wiley.com/doi/abs/10.1029/2008JE003130](https://agupubs.onlinelibrary.wiley.com/doi/abs/10.1029/2008JE003130) doi: [https://doi](https://doi.org/10.1029/2008JE003130)  
459 [.org/10.1029/2008JE003130](https://doi.org/10.1029/2008JE003130)
- 460 Chaufray, J. Y., Modolo, R., Leblanc, F., Chanteur, G., Johnson, R. E., & Luh-  
461 mann, J. G. (2007). Mars solar wind interaction: Formation of the Martian  
462 corona and atmospheric loss to space. *Journal of Geophysical Research: Planets*,  
463 112(E9). Retrieved from [https://agupubs.onlinelibrary.wiley.com/doi/abs/](https://agupubs.onlinelibrary.wiley.com/doi/abs/10.1029/2007JE002915)  
464 [10.1029/2007JE002915](https://agupubs.onlinelibrary.wiley.com/doi/abs/10.1029/2007JE002915) doi: <https://doi.org/10.1029/2007JE002915>
- 465 Chirakkil, K., Deighan, J., Lillis, R., Elliott, R., Chaffin, M., Jain, S., ... AlMazmi, H.  
466 (2022, June). More than Before: Increase in Estimated Oxygen Photochemical Escape  
467 Rates from EMM Data and Updated Modeling. In *Seventh international workshop on*  
468 *the mars atmosphere: Modelling and observations* (p. 3554).
- 469 Cravens, T. E., Hoppe, A., Ledvina, S. A., & McKenna-Lawlor, S. (2002). Pickup ions  
470 near Mars associated with escaping oxygen atoms. *Journal of Geophysical Research:*  
471 *Space Physics*, 107(A8), SMP 7-1-SMP 7-10. Retrieved from [https://agupubs](https://agupubs.onlinelibrary.wiley.com/doi/abs/10.1029/2001JA000125)  
472 [.onlinelibrary.wiley.com/doi/abs/10.1029/2001JA000125](https://agupubs.onlinelibrary.wiley.com/doi/abs/10.1029/2001JA000125) doi: [https://doi](https://doi.org/10.1029/2001JA000125)  
473 [.org/10.1029/2001JA000125](https://doi.org/10.1029/2001JA000125)
- 474 Cravens, T. E., Rahmati, A., Fox, J. L., Lillis, R., Bougher, S., Luhmann, J., ...  
475 Jakosky, B. (2017). Hot oxygen escape from Mars: Simple scaling with solar  
476 EUV irradiance. *Journal of Geophysical Research: Space Physics*, 122(1),  
477 1102-1116. Retrieved from [https://agupubs.onlinelibrary.wiley.com/doi/abs/](https://agupubs.onlinelibrary.wiley.com/doi/abs/10.1002/2016JA023461)  
478 [10.1002/2016JA023461](https://agupubs.onlinelibrary.wiley.com/doi/abs/10.1002/2016JA023461) doi: <https://doi.org/10.1002/2016JA023461>
- 479 Deighan, J., Chaffin, M., Chirakkil, K., Almatroushi, H. R., Lillis, R. J., Fillingim, M. O.,  
480 ... Chamberlin, P. C. (2022, June). Global Structure and Variability of the Inner  
481 Hot Oxygen Corona as Imaged by EMM/EMUS. In *Seventh international workshop*  
482 *on the mars atmosphere: Modelling and observations* (p. 3548).
- 483 Deighan, J., Chaffin, M. S., Chaufray, J.-Y., Stewart, A. I. F., Schneider, N. M.,  
484 Jain, S. K., ... Jakosky, B. M. (2015). MAVEN IUVS observation of  
485 the hot oxygen corona at Mars. *Geophysical Research Letters*, 42(21), 9009-  
486 9014. Retrieved from [https://agupubs.onlinelibrary.wiley.com/doi/abs/10](https://agupubs.onlinelibrary.wiley.com/doi/abs/10.1002/2015GL065487)  
487 [.1002/2015GL065487](https://agupubs.onlinelibrary.wiley.com/doi/abs/10.1002/2015GL065487) doi: <https://doi.org/10.1002/2015GL065487>
- 488 Deighan, J., Jain, S. K., Chaffin, M. S., Chaufray, J. Y., Schneider, N. M., Eparvier, F. G.,  
489 ... Lillis, R. J. (2019, July). Variability of the Martian Hot Oxygen Corona Observed  
490 by MAVEN/IUVS and Implications for Atmospheric Evolution. In LPI Editorial  
491 Board (Ed.), *Ninth international conference on mars* (Vol. 2089, p. 6383).

- 492 Eparvier, F. G., Chamberlin, P. C., Woods, T. N., & Thiemann, E. M. B. (2015, December).  
 493 The Solar Extreme Ultraviolet Monitor for MAVEN. *Space Science Reviews*, *195*(1-4),  
 494 293-301. doi: 10.1007/s11214-015-0195-2
- 495 Feldman, P. D., Steffl, A. J., Parker, J. W., A'Hearn, M. F., Bertaux, J.-L., Alan  
 496 Stern, S., ... Feaga, L. M. (2011). Rosetta-Alice observations of exospheric hy-  
 497 drogen and oxygen on Mars. *Icarus*, *214*(2), 394-399. Retrieved from [https://](https://www.sciencedirect.com/science/article/pii/S0019103511002223)  
 498 [www.sciencedirect.com/science/article/pii/S0019103511002223](https://www.sciencedirect.com/science/article/pii/S0019103511002223) doi: [https://](https://doi.org/10.1016/j.icarus.2011.06.013)  
 499 [doi.org/10.1016/j.icarus.2011.06.013](https://doi.org/10.1016/j.icarus.2011.06.013)
- 500 Fox, J. L. (1993). On the escape of oxygen and hydrogen from Mars. *Geophysical Research*  
 501 *Letters*, *20*(17), 1747-1750. Retrieved from [https://agupubs.onlinelibrary.wiley](https://agupubs.onlinelibrary.wiley.com/doi/abs/10.1029/93GL01118)  
 502 [.com/doi/abs/10.1029/93GL01118](https://agupubs.onlinelibrary.wiley.com/doi/abs/10.1029/93GL01118) doi: <https://doi.org/10.1029/93GL01118>
- 503 Fox, J. L., & Hać, A. (1997). Spectrum of hot O at the exobases of the terres-  
 504 trial planets. *Journal of Geophysical Research: Space Physics*, *102*(A11), 24005-  
 505 24011. Retrieved from [https://agupubs.onlinelibrary.wiley.com/doi/abs/10](https://agupubs.onlinelibrary.wiley.com/doi/abs/10.1029/97JA02089)  
 506 [.1029/97JA02089](https://agupubs.onlinelibrary.wiley.com/doi/abs/10.1029/97JA02089) doi: <https://doi.org/10.1029/97JA02089>
- 507 Fox, J. L., & Hać, A. B. (2009). Photochemical escape of oxygen from Mars: A com-  
 508 parison of the exobase approximation to a Monte Carlo method. *Icarus*, *204*(2),  
 509 527-544. Retrieved from [https://www.sciencedirect.com/science/article/pii/](https://www.sciencedirect.com/science/article/pii/S0019103509002917)  
 510 [S0019103509002917](https://www.sciencedirect.com/science/article/pii/S0019103509002917) doi: <https://doi.org/10.1016/j.icarus.2009.07.005>
- 511 Fox, J. L., & Hać, A. B. (2014). The escape of O from Mars: Sensitivity to the elastic cross  
 512 sections. *Icarus*, *228*, 375-385. Retrieved from [https://www.sciencedirect.com/](https://www.sciencedirect.com/science/article/pii/S0019103513004338)  
 513 [science/article/pii/S0019103513004338](https://www.sciencedirect.com/science/article/pii/S0019103513004338) doi: [https://doi.org/10.1016/j.icarus](https://doi.org/10.1016/j.icarus.2013.10.014)  
 514 [.2013.10.014](https://doi.org/10.1016/j.icarus.2013.10.014)
- 515 Fox, J. L., & Hać, A. B. (2018). Escape of O(3P), O(1D), and O(1S) from the Martian at-  
 516 mosphere. *Icarus*, *300*, 411-439. Retrieved from [https://www.sciencedirect.com/](https://www.sciencedirect.com/science/article/pii/S0019103517302026)  
 517 [science/article/pii/S0019103517302026](https://www.sciencedirect.com/science/article/pii/S0019103517302026) doi: [https://doi.org/10.1016/j.icarus](https://doi.org/10.1016/j.icarus.2017.08.041)  
 518 [.2017.08.041](https://doi.org/10.1016/j.icarus.2017.08.041)
- 519 Gröller, H., Lichtenegger, H., Lammer, H., & Shematovich, V. (2014). Hot oxygen and  
 520 carbon escape from the Martian atmosphere. *Planetary and Space Science*, *98*,  
 521 93-105. Retrieved from [https://www.sciencedirect.com/science/article/pii/](https://www.sciencedirect.com/science/article/pii/S0032063314000117)  
 522 [S0032063314000117](https://www.sciencedirect.com/science/article/pii/S0032063314000117) (Planetary evolution and life) doi: [https://doi.org/10.1016/](https://doi.org/10.1016/j.pss.2014.01.007)  
 523 [j.pss.2014.01.007](https://doi.org/10.1016/j.pss.2014.01.007)
- 524 Hodges Jr., R. R. (2000). Distributions of hot oxygen for Venus and Mars. *Journal of Geo-*  
 525 *physical Research: Planets*, *105*(E3), 6971-6981. Retrieved from [https://agupubs](https://agupubs.onlinelibrary.wiley.com/doi/abs/10.1029/1999JE001138)  
 526 [.onlinelibrary.wiley.com/doi/abs/10.1029/1999JE001138](https://agupubs.onlinelibrary.wiley.com/doi/abs/10.1029/1999JE001138) doi: [https://doi](https://doi.org/10.1029/1999JE001138)  
 527 [.org/10.1029/1999JE001138](https://doi.org/10.1029/1999JE001138)
- 528 Holsclaw, G. M., Deighan, J., Almatroushi, H., Chaffin, M., Correia, J., Evans, J. S., ...  
 529 Tyagi, K. (2021, December). The Emirates Mars Ultraviolet Spectrometer (EMUS)  
 530 for the EMM Mission. *Space Science Reviews*, *217*(8), 79. doi: 10.1007/s11214-021-  
 531 -00854-3
- 532 Huang, X., Gu, H., Cui, J., Wu, X., & Sun, M. (2022, 11). Photochemical escape of atomic  
 533 C, N, and O during the 2018 global dust storm on Mars. *Monthly Notices of the*  
 534 *Royal Astronomical Society*, *518*(4), 5982-5990. Retrieved from [https://doi.org/](https://doi.org/10.1093/mnras/stac3459)  
 535 [10.1093/mnras/stac3459](https://doi.org/10.1093/mnras/stac3459) doi: 10.1093/mnras/stac3459
- 536 Ip, W.-H. (1988). On a hot oxygen corona of Mars. *Icarus*, *76*(1), 135-145. Retrieved from  
 537 <https://www.sciencedirect.com/science/article/pii/0019103588901467> doi:  
 538 [https://doi.org/10.1016/0019-1035\(88\)90146-7](https://doi.org/10.1016/0019-1035(88)90146-7)
- 539 Ip, W.-H. (1990). The fast atomic oxygen corona extent of Mars. *Geophysical Re-*  
 540 *search Letters*, *17*(13), 2289-2292. Retrieved from [https://agupubs.onlinelibrary](https://agupubs.onlinelibrary.wiley.com/doi/abs/10.1029/GL017i013p02289)  
 541 [.wiley.com/doi/abs/10.1029/GL017i013p02289](https://agupubs.onlinelibrary.wiley.com/doi/abs/10.1029/GL017i013p02289) doi: [https://doi.org/10.1029/](https://doi.org/10.1029/GL017i013p02289)  
 542 [GL017i013p02289](https://doi.org/10.1029/GL017i013p02289)
- 543 Jain, S. K., Deighan, J., Chaffin, M., Holsclaw, G., Lillis, R., Fillingim, M., ... Eparvier,  
 544 F. (2022). Morphology of Extreme and Far Ultraviolet Martian Airglow Emissions  
 545 Observed by the EMUS Instrument on Board the Emirates Mars Mission. *Geophys-*  
 546 *ical Research Letters*, *49*(19), e2022GL099885. Retrieved from <https://agupubs>

- 547 .onlinelibrary.wiley.com/doi/abs/10.1029/2022GL099885 (e2022GL099885  
548 2022GL099885) doi: <https://doi.org/10.1029/2022GL099885>
- 549 Jain, S. K., Stewart, A. I. F., Schneider, N. M., Deighan, J., Stiepen, A., Evans, J. S., ...  
550 Jakosky, B. M. (2015). The structure and variability of Mars upper atmosphere as  
551 seen in MAVEN/IUVS dayglow observations. *Geophysical Research Letters*, *42*(21),  
552 9023-9030. Retrieved from [https://agupubs.onlinelibrary.wiley.com/doi/abs/](https://agupubs.onlinelibrary.wiley.com/doi/abs/10.1002/2015GL065419)  
553 [10.1002/2015GL065419](https://agupubs.onlinelibrary.wiley.com/doi/abs/10.1002/2015GL065419) doi: <https://doi.org/10.1002/2015GL065419>
- 554 Jakosky, B. M., Pepin, R. O., Johnson, R. E., & Fox, J. (1994). Mars Atmospheric Loss and  
555 Isotopic Fractionation by Solar-Wind-Induced Sputtering and Photochemical Escape.  
556 *Icarus*, *111*(2), 271-288. Retrieved from [https://www.sciencedirect.com/science/](https://www.sciencedirect.com/science/article/pii/S0019103584711456)  
557 [article/pii/S0019103584711456](https://www.sciencedirect.com/science/article/pii/S0019103584711456) doi: <https://doi.org/10.1006/icar.1994.1145>
- 558 Javaraiah, J. (2011). Quasi 9 and 30–40 days periodicities in the solar differential ro-  
559 tation. *Advances in Space Research*, *48*(6), 1032-1040. Retrieved from [https://](https://www.sciencedirect.com/science/article/pii/S0273117711003164)  
560 [www.sciencedirect.com/science/article/pii/S0273117711003164](https://www.sciencedirect.com/science/article/pii/S0273117711003164) doi: [https://](https://doi.org/10.1016/j.asr.2011.05.004)  
561 [doi.org/10.1016/j.asr.2011.05.004](https://doi.org/10.1016/j.asr.2011.05.004)
- 562 Kim, J., Nagy, A. F., Fox, J. L., & Cravens, T. E. (1998). Solar cycle variability of hot  
563 oxygen atoms at Mars. *Journal of Geophysical Research: Space Physics*, *103*(A12),  
564 29339-29342. Retrieved from [https://agupubs.onlinelibrary.wiley.com/doi/](https://agupubs.onlinelibrary.wiley.com/doi/abs/10.1029/98JA02727)  
565 [abs/10.1029/98JA02727](https://agupubs.onlinelibrary.wiley.com/doi/abs/10.1029/98JA02727) doi: <https://doi.org/10.1029/98JA02727>
- 566 Krestyanikova, M. A., & Shematovich, V. I. (2006, October). Stochastic models of hot  
567 planetary and satellite coronas: A hot oxygen corona of Mars. *Solar System Research*,  
568 *40*(5), 384-392. doi: 10.1134/S0038094606050030
- 569 Leblanc, F., Benna, M., Chaufray, J. Y., Martinez, A., Lillis, R., Curry, S., ...  
570 Jakosky, B. (2019). First In Situ Evidence of Mars Nonthermal Exosphere. *Geo-*  
571 *physical Research Letters*, *46*(8), 4144-4150. Retrieved from [https://agupubs](https://agupubs.onlinelibrary.wiley.com/doi/abs/10.1029/2019GL082192)  
572 [.onlinelibrary.wiley.com/doi/abs/10.1029/2019GL082192](https://agupubs.onlinelibrary.wiley.com/doi/abs/10.1029/2019GL082192) doi: [https://doi](https://doi.org/10.1029/2019GL082192)  
573 [.org/10.1029/2019GL082192](https://doi.org/10.1029/2019GL082192)
- 574 Leblanc, F., Chaufray, J. Y., Modolo, R., Leclercq, L., Curry, S., Luhmann, J., ...  
575 Jakosky, B. (2017). On the Origins of Mars' Exospheric Nonthermal Oxygen Com-  
576 ponent as Observed by MAVEN and Modeled by HELIOSARES. *Journal of Geo-*  
577 *physical Research: Planets*, *122*(12), 2401-2428. Retrieved from [https://agupubs](https://agupubs.onlinelibrary.wiley.com/doi/abs/10.1002/2017JE005336)  
578 [.onlinelibrary.wiley.com/doi/abs/10.1002/2017JE005336](https://agupubs.onlinelibrary.wiley.com/doi/abs/10.1002/2017JE005336) doi: [https://doi](https://doi.org/10.1002/2017JE005336)  
579 [.org/10.1002/2017JE005336](https://doi.org/10.1002/2017JE005336)
- 580 Leblanc, F., Martinez, A., Chaufray, J. Y., Modolo, R., Hara, T., Luhmann, J.,  
581 ... Jakosky, B. (2018). On Mars's Atmospheric Sputtering After MAVEN's  
582 First Martian Year of Measurements. *Geophysical Research Letters*, *45*(10), 4685-  
583 4691. Retrieved from [https://agupubs.onlinelibrary.wiley.com/doi/abs/10](https://agupubs.onlinelibrary.wiley.com/doi/abs/10.1002/2018GL077199)  
584 [.1002/2018GL077199](https://agupubs.onlinelibrary.wiley.com/doi/abs/10.1002/2018GL077199) doi: <https://doi.org/10.1002/2018GL077199>
- 585 Leblanc, F., Modolo, R., Curry, S., Luhmann, J., Lillis, R., Chaufray, J. Y., ...  
586 Jakosky, B. (2015). Mars heavy ion precipitating flux as measured by Mars  
587 Atmosphere and Volatile EvolutioN. *Geophysical Research Letters*, *42*(21), 9135-  
588 9141. Retrieved from [https://agupubs.onlinelibrary.wiley.com/doi/abs/10](https://agupubs.onlinelibrary.wiley.com/doi/abs/10.1002/2015GL066170)  
589 [.1002/2015GL066170](https://agupubs.onlinelibrary.wiley.com/doi/abs/10.1002/2015GL066170) doi: <https://doi.org/10.1002/2015GL066170>
- 590 Lee, Y., Combi, M. R., Tenishev, V., Bougher, S. W., Deighan, J., Schneider, N. M., ...  
591 Jakosky, B. M. (2015). A comparison of 3-D model predictions of Mars' oxygen  
592 corona with early MAVEN IUVS observations. *Geophysical Research Letters*, *42*(21),  
593 9015-9022. Retrieved from [https://agupubs.onlinelibrary.wiley.com/doi/abs/](https://agupubs.onlinelibrary.wiley.com/doi/abs/10.1002/2015GL065291)  
594 [10.1002/2015GL065291](https://agupubs.onlinelibrary.wiley.com/doi/abs/10.1002/2015GL065291) doi: <https://doi.org/10.1002/2015GL065291>
- 595 Lee, Y., Combi, M. R., Tenishev, V., Bougher, S. W., & Lillis, R. J. (2015). Hot oxygen  
596 corona at Mars and the photochemical escape of oxygen: Improved description of the  
597 thermosphere, ionosphere, and exosphere. *Journal of Geophysical Research: Planets*,  
598 *120*(11), 1880-1892. Retrieved from [https://agupubs.onlinelibrary.wiley.com/](https://agupubs.onlinelibrary.wiley.com/doi/abs/10.1002/2015JE004890)  
599 [doi/abs/10.1002/2015JE004890](https://agupubs.onlinelibrary.wiley.com/doi/abs/10.1002/2015JE004890) doi: <https://doi.org/10.1002/2015JE004890>
- 600 Lee, Y., Dong, C., Pawlowski, D., Thiemann, E., Tenishev, V., Mahaffy, P., ...  
601 Eparvier, F. (2018). Effects of a Solar Flare on the Martian Hot O

- 602 Corona and Photochemical Escape. *Geophysical Research Letters*, 45(14), 6814-  
 603 6822. Retrieved from [https://agupubs.onlinelibrary.wiley.com/doi/abs/10](https://agupubs.onlinelibrary.wiley.com/doi/abs/10.1029/2018GL077732)  
 604 .1029/2018GL077732 doi: <https://doi.org/10.1029/2018GL077732>
- 605 Lee, Y., Fang, X., Gacesa, M., Ma, Y., Tenishev, V., Mahaffy, P., ... Jakosky, B.  
 606 (2020). Effects of Global and Regional Dust Storms on the Martian Hot O Corona  
 607 and Photochemical Loss. *Journal of Geophysical Research: Space Physics*, 125(4),  
 608 e2019JA027115. Retrieved from [https://agupubs.onlinelibrary.wiley.com/doi/](https://agupubs.onlinelibrary.wiley.com/doi/abs/10.1029/2019JA027115)  
 609 [abs/10.1029/2019JA027115](https://agupubs.onlinelibrary.wiley.com/doi/abs/10.1029/2019JA027115) (e2019JA027115 2019JA027115) doi: [https://doi.org/](https://doi.org/10.1029/2019JA027115)  
 610 [10.1029/2019JA027115](https://doi.org/10.1029/2019JA027115)
- 611 Lillis, R. J., Deighan, J., Fox, J. L., Bougher, S. W., Lee, Y., Combi, M. R., ...  
 612 Chaufray, J.-Y. (2017). Photochemical escape of oxygen from Mars: First results  
 613 from MAVEN in situ data. *Journal of Geophysical Research: Space Physics*, 122(3),  
 614 3815-3836. Retrieved from [https://agupubs.onlinelibrary.wiley.com/doi/abs/](https://agupubs.onlinelibrary.wiley.com/doi/abs/10.1002/2016JA023525)  
 615 [10.1002/2016JA023525](https://agupubs.onlinelibrary.wiley.com/doi/abs/10.1002/2016JA023525) doi: [10.1002/2016JA023525](https://doi.org/10.1002/2016JA023525)
- 616 McElroy, M. B. (1972). Mars: An Evolving Atmosphere. *Science*, 175(4020), 443-445. Re-  
 617 trieved from <https://www.science.org/doi/abs/10.1126/science.175.4020.443>  
 618 doi: [10.1126/science.175.4020.443](https://doi.org/10.1126/science.175.4020.443)
- 619 McElroy, M. B., & Donahue, T. M. (1972). Stability of the Martian Atmosphere. *Science*,  
 620 177(4053), 986-988. Retrieved from [https://www.science.org/doi/abs/10.1126/](https://www.science.org/doi/abs/10.1126/science.177.4053.986)  
 621 [science.177.4053.986](https://www.science.org/doi/abs/10.1126/science.177.4053.986) doi: [10.1126/science.177.4053.986](https://doi.org/10.1126/science.177.4053.986)
- 622 Montmessin, F., Korablev, O., Lefèvre, F., Bertaux, J.-L., Fedorova, A., Trokhimovskiy,  
 623 A., ... Chapron, N. (2017). SPICAM on Mars Express: A 10 year in-depth sur-  
 624 vey of the Martian atmosphere. *Icarus*, 297, 195-216. Retrieved from [https://](https://www.sciencedirect.com/science/article/pii/S0019103516308272)  
 625 [www.sciencedirect.com/science/article/pii/S0019103516308272](https://www.sciencedirect.com/science/article/pii/S0019103516308272) doi: [https://](https://doi.org/10.1016/j.icarus.2017.06.022)  
 626 [doi.org/10.1016/j.icarus.2017.06.022](https://doi.org/10.1016/j.icarus.2017.06.022)
- 627 Nagy, A. F., & Cravens, T. E. (1988). Hot oxygen atoms in the upper atmospheres of Venus  
 628 and Mars. *Geophysical Research Letters*, 15(5), 433-435. Retrieved from [https://](https://agupubs.onlinelibrary.wiley.com/doi/abs/10.1029/GL015i005p00433)  
 629 [agupubs.onlinelibrary.wiley.com/doi/abs/10.1029/GL015i005p00433](https://agupubs.onlinelibrary.wiley.com/doi/abs/10.1029/GL015i005p00433) doi:  
 630 <https://doi.org/10.1029/GL015i005p00433>
- 631 Nier, A. O., & McElroy, M. B. (1977). Composition and structure of Mars' Upper at-  
 632 mosphere: Results from the neutral mass spectrometers on Viking 1 and 2. *Journal*  
 633 *of Geophysical Research (1896-1977)*, 82(28), 4341-4349. Retrieved from [https://](https://agupubs.onlinelibrary.wiley.com/doi/abs/10.1029/JS082i028p04341)  
 634 [agupubs.onlinelibrary.wiley.com/doi/abs/10.1029/JS082i028p04341](https://agupubs.onlinelibrary.wiley.com/doi/abs/10.1029/JS082i028p04341) doi:  
 635 <https://doi.org/10.1029/JS082i028p04341>
- 636 Petrigiani, A., van der Zande, W. J., Cosby, P. C., Hellberg, F., Thomas, R. D., & Larsson,  
 637 M. (2004, 12). Vibrationally resolved rate coefficients and branching fractions in the  
 638 dissociative recombination of O<sub>2</sub><sup>+</sup>. *The Journal of Chemical Physics*, 122(1), 014302.  
 639 Retrieved from <https://doi.org/10.1063/1.1825991> doi: [10.1063/1.1825991](https://doi.org/10.1063/1.1825991)
- 640 Qin, J., Liu, H., & Xu, Z. (2024). Mars Hot Oxygen Density and Effective Temperature  
 641 Derived From the MAVEN IUVS Observations. *Journal of Geophysical Research:*  
 642 *Planets*, 129(1), e2023JE007853. Retrieved from [https://agupubs.onlinelibrary](https://agupubs.onlinelibrary.wiley.com/doi/abs/10.1029/2023JE007853)  
 643 [.wiley.com/doi/abs/10.1029/2023JE007853](https://agupubs.onlinelibrary.wiley.com/doi/abs/10.1029/2023JE007853) (e2023JE007853 2023JE007853) doi:  
 644 <https://doi.org/10.1029/2023JE007853>
- 645 Rahmati, A., Larson, D. E., Cravens, T. E., Lillis, R. J., Dunn, P. A., Halekas, J. S.,  
 646 ... Jakosky, B. M. (2015). MAVEN insights into oxygen pickup ions at Mars.  
 647 *Geophysical Research Letters*, 42(21), 8870-8876. Retrieved from [https://agupubs](https://agupubs.onlinelibrary.wiley.com/doi/abs/10.1002/2015GL065262)  
 648 [.onlinelibrary.wiley.com/doi/abs/10.1002/2015GL065262](https://agupubs.onlinelibrary.wiley.com/doi/abs/10.1002/2015GL065262) doi: [https://doi](https://doi.org/10.1002/2015GL065262)  
 649 [.org/10.1002/2015GL065262](https://doi.org/10.1002/2015GL065262)
- 650 Rahmati, A., Larson, D. E., Cravens, T. E., Lillis, R. J., Halekas, J. S., McFadden,  
 651 J. P., ... Jakosky, B. M. (2017). MAVEN measured oxygen and hydrogen pickup  
 652 ions: Probing the Martian exosphere and neutral escape. *Journal of Geophys-*  
 653 *ical Research: Space Physics*, 122(3), 3689-3706. Retrieved from [https://agupubs](https://agupubs.onlinelibrary.wiley.com/doi/abs/10.1002/2016JA023371)  
 654 [.onlinelibrary.wiley.com/doi/abs/10.1002/2016JA023371](https://agupubs.onlinelibrary.wiley.com/doi/abs/10.1002/2016JA023371) doi: [https://doi](https://doi.org/10.1002/2016JA023371)  
 655 [.org/10.1002/2016JA023371](https://doi.org/10.1002/2016JA023371)
- 656 Rahmati, A., Larson, D. E., Cravens, T. E., Lillis, R. J., Halekas, J. S., McFadden, J. P., ...

- 657 Jakosky, B. M. (2018). Seasonal Variability of Neutral Escape from Mars as Derived  
 658 From MAVEN Pickup Ion Observations. *Journal of Geophysical Research: Planets*,  
 659 *123*(5), 1192-1202. Retrieved from [https://agupubs.onlinelibrary.wiley.com/](https://agupubs.onlinelibrary.wiley.com/doi/abs/10.1029/2018JE005560)  
 660 [doi: https://doi.org/10.1029/2018JE005560](https://doi.org/10.1029/2018JE005560)
- 661 Ramstad, R., Brain, D. A., Dong, Y., Halekas, J. S., McFadden, J. M., Mitchell, D. L.,  
 662 ... Jakosky, B. M. (2023). Solar wind driven influences on the Martian oxygen  
 663 corona: Constraints on atmospheric sputtering from a synthesis of MAVEN mea-  
 664 surements during solar minimum. *Icarus*, *397*, 115491. Retrieved from [https://](https://www.sciencedirect.com/science/article/pii/S0019103523000684)  
 665 [www.sciencedirect.com/science/article/pii/S0019103523000684](https://www.sciencedirect.com/science/article/pii/S0019103523000684) doi: [https://](https://doi.org/10.1016/j.icarus.2023.115491)  
 666 [doi.org/10.1016/j.icarus.2023.115491](https://doi.org/10.1016/j.icarus.2023.115491)
- 667 Shematovich, V. I. (2013, November). Suprathermal oxygen and hydrogen atoms in the  
 668 upper Martian atmosphere. *Solar System Research*, *47*(6), 437-445. doi: 10.1134/  
 669 S0038094613060087
- 670 Shematovich, V. I. (2021, July). Atmospheric Loss of Atomic Oxygen during Proton Aurorae  
 671 on Mars. *Solar System Research*, *55*(4), 324-334. doi: 10.1134/S0038094621040079
- 672 Strickland, D. J., Stewart, A. I., Barth, C. A., Hord, C. W., & Lane, A. L.  
 673 (1973). Mariner 9 Ultraviolet Spectrometer Experiment: Mars atomic oxygen  
 674 1304-A emission. *Journal of Geophysical Research (1896-1977)*, *78*(22), 4547-  
 675 4559. Retrieved from [https://agupubs.onlinelibrary.wiley.com/doi/abs/10](https://agupubs.onlinelibrary.wiley.com/doi/abs/10.1029/JA078i022p04547)  
 676 [.1029/JA078i022p04547](https://doi.org/10.1029/JA078i022p04547) doi: <https://doi.org/10.1029/JA078i022p04547>
- 677 Strickland, D. J., Thomas, G. E., & Sparks, P. R. (1972). Mariner 6 and 7 Ultraviolet Spec-  
 678 trometer Experiment: Analysis of the O I 1304- and 1356-A emissions. *Journal of Geo-*  
 679 *physical Research (1896-1977)*, *77*(22), 4052-4068. Retrieved from [https://agupubs](https://agupubs.onlinelibrary.wiley.com/doi/abs/10.1029/JA077i022p04052)  
 680 [.onlinelibrary.wiley.com/doi/abs/10.1029/JA077i022p04052](https://doi.org/10.1029/JA077i022p04052) doi: [https://](https://doi.org/10.1029/JA077i022p04052)  
 681 [doi.org/10.1029/JA077i022p04052](https://doi.org/10.1029/JA077i022p04052)
- 682 Thiemann, E. M. B., Chamberlin, P. C., Eparvier, F. G., Templeman, B., Woods, T. N.,  
 683 Bougher, S. W., & Jakosky, B. M. (2017). The MAVEN EUVM model of solar  
 684 spectral irradiance variability at Mars: Algorithms and results. *Journal of Geophysi-*  
 685 *cal Research: Space Physics*, *122*(3), 2748-2767. Retrieved from [https://agupubs](https://agupubs.onlinelibrary.wiley.com/doi/abs/10.1002/2016JA023512)  
 686 [.onlinelibrary.wiley.com/doi/abs/10.1002/2016JA023512](https://doi.org/10.1002/2016JA023512) doi: [https://doi](https://doi.org/10.1002/2016JA023512)  
 687 [.org/10.1002/2016JA023512](https://doi.org/10.1002/2016JA023512)
- 688 Yagi, M., Leblanc, F., Chaufray, J., Gonzalez-Galindo, F., Hess, S., & Modolo, R. (2012).  
 689 Mars exospheric thermal and non-thermal components: Seasonal and local varia-  
 690 tions. *Icarus*, *221*(2), 682-693. Retrieved from [https://www.sciencedirect.com/](https://www.sciencedirect.com/science/article/pii/S0019103512002989)  
 691 [science/article/pii/S0019103512002989](https://doi.org/10.1016/j.icarus.2012.07.022) doi: [https://doi.org/10.1016/j.icarus](https://doi.org/10.1016/j.icarus.2012.07.022)  
 692 [.2012.07.022](https://doi.org/10.1016/j.icarus.2012.07.022)
- 693 Zhang, Q., Gu, H., Cui, J., Cheng, Y. M., He, Z. G., Zhong, J. H., ... Wei, Y. (2020,  
 694 February). Atomic Oxygen Escape on Mars Driven by Electron Impact Excitation and  
 695 Ionization. *The Astronomical Journal*, *159*(2), 54. doi: 10.3847/1538-3881/ab6297